Power Beacon-Assisted Energy Harvesting in a Half-Duplex Communication Network under Co-Channel Interference over a Rayleigh Fading Environment: Energy Efficiency and Outage Probability Analysis

Van-Duc Phan [1], Tan N. Nguyen [2,*] , Minh Tran [3] , Tran Thanh Trang [4], Miroslav Voznak [5] , Duy-Hung Ha [2,5] and Thanh-Long Nguyen [6]

[1] Center of Excellence for Automation and Precision Mechanical Engineering, Nguyen Tat Thanh University, Ho Chi Minh City 70000, Vietnam
[2] Wireless Communications Research Group, Faculty of Electrical & Electronics Engineering, Ton Duc Thang University, 19 Nguyen Huu Tho Street, Ho Chi Minh City 70000, Vietnam
[3] Optoelectronics Research Group, Faculty of Electrical and Electronics Engineering, Ton Duc Thang University, Ho Chi Minh City 70000, Vietnam
[4] National Key Laboratory of Digital Control and System Engineering, Ho Chi Minh City 70000, Vietnam
[5] Faculty of Electrical Engineering and Computer Science, Technical University of Ostrava, Ostrava 70833, Czech Republic
[6] Center for Information Technology, Ho Chi Minh City University of Food Industry, Ho Chi Minh City 70000, Vietnam
* Correspondence: nguyennhattan@tdtu.edu.vn

Abstract: In this time, energy efficiency (EE), measured in bits per Watt, has been considered as an important emerging metric in energy-constrained wireless communication networks because of their energy shortage. In this paper, we investigate power beacon assisted (PB) energy harvesting (EH) in half-duplex (HD) communication network under co-channel Interferer over Rayleigh fading environment. In this work, we investigate the model system with the time switching (TS) protocol. Firstly, the exact and asymptotic form expressions of the outage probability (OP) are analyzed and derived. Then the system EE is investigated and the influence of the primary system parameters on the system performance. Finally, we verify the correctness of the analytical expressions using Monte Carlo simulation. Finally, we can state that the simulation and analytical results are the same.

Keywords: power beacon (PB); energy efficiency (EE); outage probability (OP); energy harvesting (EH); co-channel interference (CCI)

1. Introduction

Nowadays, the Internet of Things (IoT) is considered to be a hot research topic. In this network, all smart devices can work and cooperate over the Internet environment. The links between the digital and real worlds help smart devices to react like humans (smart devices can hear, see, think, make decisions, and perform complicated tasks). The critical advantage of the IoT is that smart devices can automatically do their tasks without human involvement. Nowadays, the IoT is involved in all aspects of civilian life, including transportation, smart grids, security and public safety, agriculture, logistics, and e-health. Furthermore, energy harvesting (EH), in which radio frequency (RF) signals can transfer both information and energy at the same time, can be considered to be a promising solution

for extending the lifetime of energy-constrained IoT devices [1–10]. EH communication systems commonly use the two traditional time switching (TS) and power splitting (PS) protocols, with the comparison of these protocols in different system networks. Moreover, we can see that the loss of information in the harvesting phase in the TS protocol and the low coverage area in the PS protocol are the main disadvantages of these protocols. In addition, the complicated hardware structure of the PS protocol compared with the simpler hardware in the TS protocol is also a main disadvantage of the PS protocol. [11–16]. In this research, we selected the half-duplex (HD) model because of its simplicity and the possibility of applying it in real-world scenarios. In reality, not all wireless nodes are equipped with full-duplex capacity due to limitations in hardware or implementation cost. From this point of view, we considered the TS protocol and the HD model for our model system.

In the next generation of communication systems, billions of wireless devices will be connected to each other via the IoT system, which will lead to an energy consumption problem. Therefore, energy efficiency (EE), measured in bits per watt, is considered to be an important emerging metric in energy-constrained wireless communication networks due to their energy shortage [17–19]. The authors of [20] investigated the EE optimization problems in the SWIPT sensor networks, which employs both the PS and the TS protocols. In [21], the authors investigated an EE resource allocation algorithm for SWIPT in an OFDMA system, where the receivers employed the PS scheme to harvest energy. The authors of [22] investigated OFDMA systems with the PS SWIPT, and proposed a resource allocation (ResAll) scheme to maximize EE. Without considering SWIPT, for the MIMO two-way AF relay channels, the latest EE beamforming scheme was derived in [23], which only considers a single-stream transmission per user and cannot be applied to multiple data stream scenarios because of the different objective expressions. In [24], the optimal global EE performance was investigated in interference-limited networks where the SWIPT scheme was not employed. The EE in SWIPT is based on the IoT distributed antenna system (DAS), as studied in [25]. In [26], a time-slotted large-scale MIMO system for energy harvesting and information transmission was studied, where an energy-efficient optimization scheme was proposed by jointly optimizing both transfer duration and transmitted power. The authors of [27] developed a distributed iteration algorithm for power allocation, PS ratio, and relay selection to maximize EE in clustered wireless sensor networks with SWIPT. The authors of [28] considered the EE maximization problem in a wireless powered communication network (WPCN), where multiple users harvest energy from a dedicated power station and then communicate with an information receiving station.

In this research, we propose and investigate power beacon-assisted (PB) EH in an HD communication network under co-channel interference over a Rayleigh fading environment. We considered the model system to be the TS protocol. Firstly, the exact and asymptotic form expressions of the outage probability (OP) were derived. Then we investigated the EE of the model system and the influence of the primary system parameters on the performance of the proposed system. Finally, the accuracy of the analytical expressions was derived and verified using a Monte Carlo simulation in connection with the primary system parameters. From the results, we determined that the analytical mathematical and simulated results are the same. The main contributions are summarized as follows:

1. The system model of a PB EH in an HD communication network under co-channel interference over a Rayleigh fading environment.
2. The exact and asymptotic form expressions of the OP were derived.
3. The EE of the model system and the influence of the primary system parameters on the performance of the proposed system were investigated.
4. A Monte Carlo simulation was conducted to verify the analysis results using the primary system parameters.

The rest of this paper is organized as follows. Section 2 presents the system model. Section 3 investigates the system performance and the system EE. Section 4 gives the results, and some discussions are provided. Finally, some conclusions are drawn in Section 5.

2. System Model

In this work, we consider a PB EH in an HD communication network. From Figure 1, we denote that S and D are the source node and the destination node, respectively, PB denotes a power beacon-assisted node, and I denotes the co-channel interference from the environment. Let f_1 and f_2 represent the I-S and I-D interference channels, respectively. Let h and g denote the PB-S and S-D channels. Assume that all channels are Rayleigh block fading channels. As drawn in Figure 2, the whole transmission block (T) can be divided into parts. Let T and $0 < \alpha < 1$ denote the whole symbol duration and the TS factor, respectively. S and I scavenge energy from the radio frequency signal received from the PB node S and node I, respectively, during αT. Moreover, the remaining $(1 - \alpha)$T is spent on signal transmission from node S to node D, and the signal from node I to node D. Note that all the energy harvested at node S and node I is consumed for forwarding source information to node D.
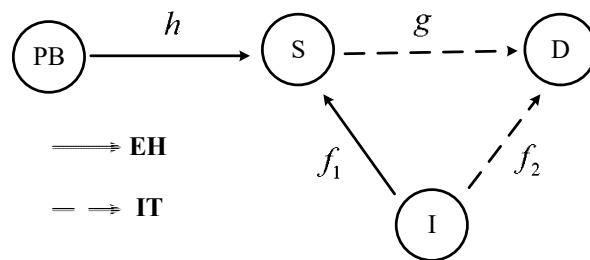
Figure 1. System model. PB, power beacon-assisted node; EH, energy harvesting; I, co-channel interference from the environment; IT, information transmission; S, source node; D, destination node; f_1, I-S interference channel; f_2, I-D interference channel; h, PB-S channel; g, S-D channel.
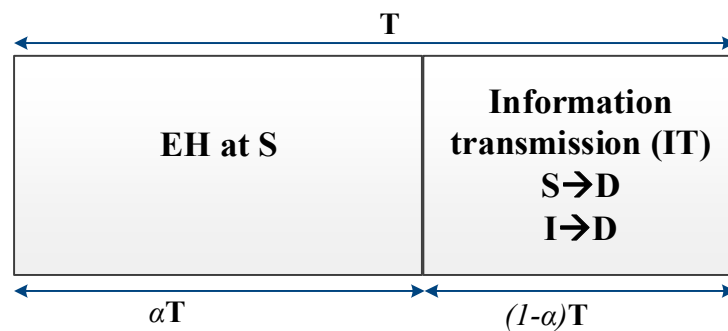
Figure 2. EH and information processing. T, the whole transmission block.

2.1. Energy Harvesting

In the first phase, the received signal at node S during the EH phase is formulated as:

$$y_s = hx_b + f_1 s_i + n_s \tag{1}$$

where x_b is the transmit signal at the PB, $\mathrm{E}\{|x_b|^2\} = P_B$, $\mathrm{E}\{\bullet\}$ is the expectation operator, P_B is the transmit power of the power beacon, n_s is the additive white Gaussian noise (AWGN) with zero-mean and variance N_0, S_i is the transmit signal at the interferer, $\mathrm{E}\{|s_i|^2\} = P_I$, and P_I is the transmit power of the interferer.

The total received energy during the first phase at node S is formulated as:

$$E_s = \eta_B |h|^2 P_B \alpha T + \eta_I |f_1|^2 P_I \alpha T \tag{2}$$

where $0 < \{\eta_B, \eta_I\} < 1$ is the energy conversion efficiency of the PB and the interferer, respectively.

We assume that $\eta_B = \eta_I = \eta$. Hence, the average transmit power at node S could be obtained by the following equation:

$$P_s = \frac{E_s}{(1-\alpha)T} = \frac{\eta|h|^2 P_B \alpha T + \eta|f_1|^2 P_I \alpha T}{(1-\alpha)T} = \kappa\left(P_B|h|^2 + |f_1|^2 P_I\right) \tag{3}$$

where $\kappa = \frac{\eta\alpha}{1-\alpha}$.

2.2. Information Transmission

In the second phase, node S transmits the signal to node D, and the received signal, y_D, at the destination is formulated as:

$$y_D = gx_s + f_2 s_i + n_d = \underbrace{gx_s}_{signal} + \underbrace{f_2 s_i + n_d}_{noise} \tag{4}$$

where we have $E\{|x_s|^2\} = P_s$, and n_d is the AWGN with zero-mean and variance N_0.

From Equation (4), the end to end signal to interference plus noise ratio (SINR) was calculated as the following:

$$\gamma_{e2e} = \frac{E\{|signal|^2\}}{E\{|noise|^2\}} = \frac{|g|^2 P_s}{|f_2|^2 P_I + N_0}. \tag{5}$$

Substituting Equation (3) into Equation (5) and assuming that the power of interferer noise is very large, so $P_B \approx P_I$, we have:

$$\gamma_{e2e} = \frac{\kappa|g|^2\left(P_B|h|^2 + |f_1|^2 P_I\right)}{|f_2|^2 P_I + N_0} = \frac{\kappa|g|^2\Delta\left(|h|^2 + |f_1|^2\right)}{|f_2|^2\Delta + 1} \tag{6}$$

where $\Delta = \frac{P_B}{N_0} = \frac{P_I}{N_0}$.

3. The System Performance

3.1. Outage Probability

Based on the system model in the above section, we derived the OP throughput performance and EE of the proposed system.

From Equation (6) we obtain the OP of the model system as the following:

$$\begin{aligned} OP &= \Pr(\gamma_{e2e} < \gamma_0) = \Pr\left[\frac{\kappa|g|^2\Delta\left(|h|^2 + |f_1|^2\right)}{|f_2|^2\Delta + 1} < \gamma_0\right] \\ &= \Pr(XY < \gamma_0) = \int_0^\infty F_Y\left(\frac{\gamma_0}{X}\Big|X = x\right)f_X(x)dx \end{aligned} \tag{7}$$

where $\gamma_0 = 2^{2R} - 1$ is the threshold of the system, R is the source rate, $X = |h|^2 + |f_1|^2 = \varphi_1 + \varphi_2$, $Y = \frac{\kappa|g|^2\Delta}{|f_2|^2\Delta + 1} = \frac{\kappa\varphi_3\Delta}{1 + \Delta\varphi_4}$, and $\varphi_1 = |h|^2$, $\varphi_2 = |f_1|^2$, $\varphi_3 = |g|^2$, $\varphi_4 = |f_2|^2$.

In order to calculate the probability in Equation (7), we have to determine the probability density function (PDF) and the cumulative density function (CDF) of X and Y, respectively, as in Lemma 1 and Lemma 2.

Lemma 1. *The CDF of Y can be computed as:*

$$
\begin{aligned}
F_Y(a) \quad &= \Pr(Y < a) \; = \; \Pr\!\left(\frac{\kappa\varphi_3\Delta}{1+\Delta\varphi_4} < a\right) \; = \; \Pr\!\left(\varphi_3 < \frac{a}{\kappa\Delta} + \frac{a\varphi_4}{\kappa}\right) \\
&= \int_0^\infty f_{\varphi_4}(\varphi_4)d\varphi_4 \int_0^{\frac{a}{\kappa\Delta}+\frac{a\varphi_4}{\kappa}} f_{\varphi_3}(\varphi_3)d\varphi_3 \; = \; \int_0^\infty F_{\varphi_3}\!\left(\frac{a}{\kappa\Delta} + \frac{a\varphi_4}{\kappa}\right)f_{\varphi_4}(\varphi_4)d\varphi_4 \\
&= \int_0^\infty f_{\varphi_4}(\varphi_4)d\varphi_4 - \frac{1}{\lambda_4}\int_0^\infty \exp\!\left(-\frac{a}{\kappa\Delta\lambda_3} - \frac{a\varphi_4}{\kappa\lambda_3}\right)\exp\!\left(-\frac{\varphi_4}{\lambda_4}\right)d\varphi_4 \\
&= 1 - \frac{\kappa\lambda_3 \exp\!\left(-\frac{a}{\kappa\Delta\lambda_3}\right)}{a\lambda_4 + \kappa\lambda_3}
\end{aligned}
\tag{8}
$$

where λ_3, λ_4 are the mean of the random variables (RVs) φ_3, φ_4, respectively.

Lemma 2. *The CDF of X can be expressed as:*

$$
\begin{aligned}
F_X(a) = \quad &\Pr[(\varphi_1 + \varphi_2) < a] \; = \; \Pr[\varphi_1 < a - \varphi_2] \\
&= \int_0^a f_{\varphi_2}(\varphi_2)d\varphi_2 \int_0^{a-\varphi_2} f_{\varphi_1}(\varphi_1)d\varphi_1 \; = \; \int_0^a F_{\varphi_1}(a - \varphi_2)f_{\varphi_2}(\varphi_2)d\varphi_2 \\
&= \frac{1}{\lambda_2}\int_0^a\left[1 - \exp\!\left(-\frac{a-\varphi_2}{\lambda_1}\right)\right]\exp\!\left(-\frac{\varphi_2}{\lambda_2}\right)d\varphi_2 \\
&= 1 - \exp\!\left(-\frac{a}{\lambda_2}\right) - \frac{\exp\!\left(-\frac{a}{\lambda_1}\right)}{\lambda_2}\int_0^a \exp\!\left(\varphi_2\left[\frac{1}{\lambda_1} - \frac{1}{\lambda_2}\right]\right)d\varphi_2
\end{aligned}
\tag{9}
$$

where λ_1, λ_2 are the mean of the RVs φ_1, φ_2, respectively.

In this situation, we investigated two cases as follows:

Case 1: *We assume that $\lambda_1 = \lambda_2 = \lambda$.*

From Equation (9), we obtain:

$$
F_X(a) \; = \; 1 - \exp\!\left(-\frac{a}{\lambda}\right) - \frac{a\exp\!\left(-\frac{a}{\lambda}\right)}{\lambda}.
\tag{10}
$$

Therefore, the PDF can be obtained as:

$$
f_X(a) \; = \; \frac{\partial F_X(a)}{\partial a} \; = \; \frac{a\exp\!\left(-\frac{a}{\lambda}\right)}{\lambda^2}
\tag{11}
$$

Case 2: *We assume that $\lambda_1 \neq \lambda_2$.*

Similarly, we can obtain the CDF and the PDF of X as follows:

$$
F_X(a) \; = \; 1 - \exp\!\left(-\frac{a}{\lambda_2}\right) - \frac{\lambda_1}{\lambda_2 - \lambda_1}\left[\exp\!\left(-\frac{a}{\lambda_2}\right) - \exp\!\left(-\frac{a}{\lambda_1}\right)\right].
\tag{12}
$$

$$
f_X(a) \; = \; \frac{1}{\lambda_2 - \lambda_1}\left[\exp\!\left(-\frac{a}{\lambda_2}\right) - \exp\!\left(-\frac{a}{\lambda_1}\right)\right].
\tag{13}
$$

3.1.1. Exact Analysis

Case 1: $\lambda_1 = \lambda_2 = \lambda$.

Combining Equation (8), Equation (11) and applying them to Equation (7) allows the OP to be computed as:

$$
\begin{aligned}
OP_1 &= \int_0^\infty F_Y\left(\frac{\gamma_0}{X}\Big|X = x\right)f_X(x)dx = 1 - \int_0^\infty \frac{\kappa\lambda_3\exp\left(-\frac{\gamma_0}{x\kappa\Delta\lambda_3}\right)}{\frac{\gamma_0}{x}\lambda_4+\kappa\lambda_3} \times \frac{x\exp\left(-\frac{x}{\lambda}\right)}{\lambda^2}dx \\
&= 1 - \frac{\kappa\lambda_3}{\lambda^2}\int_0^\infty \frac{x^2}{\kappa\lambda_3 x+\gamma_0\lambda_4} \times \exp\left(-\frac{\gamma_0}{\kappa\Delta\lambda_3 x}\right) \times \exp\left(-\frac{x}{\lambda}\right)dx
\end{aligned}
\tag{14}
$$

Case 2: $\lambda_1 \neq \lambda_2$.

Combining Equation (8) and Equation (13), we can obtain the OP, in this case as follows:

$$
\begin{aligned}
OP_2 &= 1 - \int_0^\infty \frac{\kappa\lambda_3\exp\left(-\frac{\gamma_0}{x\kappa\Delta\lambda_3}\right)}{\frac{\gamma_0}{x}\lambda_4+\kappa\lambda_3} \times \left\{\frac{1}{\lambda_2-\lambda_1}\left[\exp\left(-\frac{x}{\lambda_2}\right)-\exp\left(-\frac{x}{\lambda_1}\right)\right]\right\}dx \\
&= 1 - \frac{\kappa\lambda_3}{\lambda_2-\lambda_1}\int_0^\infty \frac{x\exp\left(-\frac{\gamma_0}{\kappa\Delta\lambda_3 x}\right)}{\kappa\lambda_3 x+\gamma_0\lambda_4} \times \left\{\exp\left(-\frac{x}{\lambda_2}\right)-\exp\left(-\frac{x}{\lambda_1}\right)\right\}dx
\end{aligned}
\tag{15}
$$

3.1.2. Asymptotic Analysis

The high SINR regime and the end to end SINR from Equation (6) can be approximated as:

$$
\gamma_{e2e}^\infty \approx \frac{\kappa|g|^2\left(|h|^2 + |f_1|^2\right)}{|f_2|^2} = ZX
\tag{16}
$$

where $X = |h|^2 + |f_1|^2 = \varphi_1 + \varphi_2$, $Z = \frac{\kappa|g|^2}{|f_2|^2} = \frac{\kappa\varphi_3}{\varphi_4}$.

Lemma 3. *The CDF of Z can be calculated using the equation:*

$$
\begin{aligned}
F_Z(a) &= \Pr(Z < a) = \Pr\left(\frac{\kappa\varphi_3}{\varphi_4} < a\right) = \Pr\left(\varphi_3 < \frac{a\varphi_4}{\kappa}\right) \\
&= \int_0^\infty f_{\varphi_4}(\varphi_4)d\varphi_4 \int_0^{\frac{a\varphi_4}{\kappa}} f_{\varphi_3}(\varphi_3)d\varphi_3 \\
&= 1 - \frac{1}{\lambda_4}\int_0^\infty \exp\left(-\frac{a\varphi_4}{\kappa\lambda_3}\right) \times \exp\left(-\frac{\varphi_4}{\lambda_4}\right)d\varphi_4 \\
&= 1 - \frac{\kappa\lambda_3}{a\lambda_4+\kappa\lambda_3}
\end{aligned}
\tag{17}
$$

Case 1: $\lambda_1 = \lambda_2 = \lambda$.

From Equations (11), (16), and (17), the OP can be computed as:

$$
\begin{aligned}
OP_1^\infty &= \Pr\left(\gamma_{e2e}^\infty < \gamma_0\right) = \Pr\left[\frac{\kappa|g|^2\left(|h|^2+|f_1|^2\right)}{|f_2|^2} < \gamma_0\right] \\
&= \Pr(XZ < \gamma_0) = \int_0^\infty F_Z\left(\frac{\gamma_0}{X}\Big|X = x\right)f_X(x)dx \\
&= 1 - \frac{1}{\lambda^2}\int_0^\infty \frac{x^2}{x+\frac{\gamma_0\lambda_4}{\kappa\lambda_3}} \times \exp\left(-\frac{x}{\lambda}\right)dx
\end{aligned}
\tag{18}
$$

Applying Equation (3.353,5) from the table of integrals [29], Equation (18) can be rewritten as:

$$OP_1^\infty = \frac{\gamma_0 \lambda_4 \lambda}{\kappa \lambda_3} + \left(\frac{\gamma_0 \lambda_4}{\kappa \lambda_3 \lambda}\right)^2 \exp\left(\frac{\gamma_0 \lambda_4}{\kappa \lambda_3 \lambda}\right) \text{Ei}\left(-\frac{\gamma_0 \lambda_4}{\kappa \lambda_3 \lambda}\right) \tag{19}$$

where $\text{Ei}(-z) = -\int\limits_z^\infty e^{-t} t^{-1} dt$ is the exponential integral function.

Case 2: $\lambda_1 \neq \lambda_2$.

In this case, based on Equations (13), (16), and (17), the OP can be calculated as:

$$\begin{aligned}
OP_2^\infty &= 1 - \frac{1}{\lambda_2 - \lambda_1} \int\limits_0^\infty \frac{x}{x + \frac{\gamma_0 \lambda_4}{\kappa \lambda_3}} \times \left\{\exp\left(-\frac{x}{\lambda_2}\right) - \exp\left(-\frac{x}{\lambda_1}\right)\right\} dx \\
&= 1 - \frac{1}{\lambda_2 - \lambda_1} \int\limits_0^\infty \frac{x \exp\left(-\frac{x}{\lambda_2}\right)}{x + \frac{\gamma_0 \lambda_4}{\kappa \lambda_3}} dx + \frac{1}{\lambda_2 - \lambda_1} \int\limits_0^\infty \frac{x \exp\left(-\frac{x}{\lambda_1}\right)}{x + \frac{\gamma_0 \lambda_4}{\kappa \lambda_3}} dx.
\end{aligned} \tag{20}$$

Similar to the previous case, we apply Equation (3.353,5) from the table of integrals [29], thus Equation (19) can be formulated as follows:

$$\begin{aligned}
OP_2^\infty &= 1 - \frac{\gamma_0 \lambda_4}{\kappa \lambda_3 (\lambda_2 - \lambda_1)} \exp\left(\frac{\gamma_0 \lambda_4}{\kappa \lambda_3 \lambda_2}\right) \text{Ei}\left(-\frac{\gamma_0 \lambda_4}{\kappa \lambda_3 \lambda_2}\right) - \frac{\lambda_2}{\lambda_2 - \lambda_1} \\
&\quad + \frac{\gamma_0 \lambda_4}{\kappa \lambda_3 (\lambda_2 - \lambda_1)} \exp\left(\frac{\gamma_0 \lambda_4}{\kappa \lambda_3 \lambda_1}\right) \text{Ei}\left(-\frac{\gamma_0 \lambda_4}{\kappa \lambda_3 \lambda_1}\right) + \frac{\lambda_1}{\lambda_2 - \lambda_1} \\
&= \frac{\gamma_0 \lambda_4}{\kappa \lambda_3 (\lambda_2 - \lambda_1)} \left\{\exp\left(\frac{\gamma_0 \lambda_4}{\kappa \lambda_3 \lambda_1}\right) \text{Ei}\left(-\frac{\gamma_0 \lambda_4}{\kappa \lambda_3 \lambda_1}\right) - \exp\left(\frac{\gamma_0 \lambda_4}{\kappa \lambda_3 \lambda_2}\right) \text{Ei}\left(-\frac{\gamma_0 \lambda_4}{\kappa \lambda_3 \lambda_2}\right)\right\}
\end{aligned} \tag{21}$$

3.2. Energy Efficiency Analysis

The EE is defined as a ratio of total information rate C and total power consumption E_T in [18]:

$$EE = \frac{C}{E_T} \tag{22}$$

where $C = \frac{(1-\alpha)T}{2} \log_2(1 + \gamma_{e2e})$ and $E_T = [2\alpha T + (1-\alpha)T]\frac{P}{\varepsilon} + P_C T$, in which $P = P_B = P_I$, and ε and P_C denote the power amplifier efficiency of the power beacon and circuit power consumption, respectively.

Finally, we obtain the *EE* as shown in the equation below:

$$EE = \frac{\frac{(1-\alpha)}{2} \log_2(1 + \gamma_{e2e})}{(T + \alpha T)P/\varepsilon + P_C T} = \frac{\frac{(1-\alpha)}{2} \log_2(1 + \gamma_{e2e})}{(1+\alpha)P/\varepsilon + P_C}. \tag{23}$$

In order to analyze the EE, we considered calculating the average total information rate in two cases: $\lambda_1 = \lambda_2 = \lambda$ and $\lambda_1 \neq \lambda_2$.

The average total information rate can be expressed as [30]:

$$C_{avg} = \frac{(1-\alpha)}{2 \ln 2} \int\limits_0^\infty \frac{1 - F_{\gamma_{e2e}}(\gamma_0)}{1 + \gamma_0} d\gamma_0. \tag{24}$$

Case 1: $\lambda_1 = \lambda_2 = \lambda$.

a. Exact Analysis

Substituting Equation (14) into Equation (24), we obtain C_{avg} as follows:

$$
\begin{aligned}
C_{1\_avg} &= \frac{(1-\alpha)}{2\ln 2}\int_0^\infty \frac{1-F_{\gamma_{e2e}}(\gamma_0)}{1+\gamma_0}d\gamma_0 \\
&= \frac{(1-\alpha)\kappa\lambda_3}{2\lambda^2\ln 2}\int_0^\infty\int_0^\infty \frac{x^2}{(\kappa\lambda_3 x+\gamma_0\lambda_4)(1+\gamma_0)}\times\exp\left(-\frac{\gamma_0}{\kappa\Delta\lambda_3 x}\right)\times\exp\left(-\frac{x}{\lambda}\right)dxd\gamma_0
\end{aligned}
\tag{25}
$$

Next, substituting Equation (25) into Equation (22), finally, the average EE can be given as:

$$
EE_{1\_avg} = \frac{\frac{(1-\alpha)\kappa\lambda_3}{2\lambda^2\ln 2}\int_0^\infty\int_0^\infty \frac{x^2}{(\kappa\lambda_3 x+\gamma_0\lambda_4)(1+\gamma_0)}\times\exp\left(-\frac{\gamma_0}{\kappa\Delta\lambda_3 x}\right)\times\exp\left(-\frac{x}{\lambda}\right)dxd\gamma_0}{(1+\alpha)P/\varepsilon+P_C}.
\tag{26}
$$

b. Asymptotic Analysis

Substituting Equation (19) into Equation (24), the average total information rate can be expressed as:

$$
C_{1\_avg}^\infty = \frac{(1-\alpha)}{2\ln 2}\int_0^\infty\left[1-\left\{\frac{\gamma_0\lambda_4\lambda}{\kappa\lambda_3}+\left(\frac{\gamma_0\lambda_4}{\kappa\lambda_3\lambda}\right)^2\exp\left(\frac{\gamma_0\lambda_4}{\kappa\lambda_3\lambda}\right)\mathrm{Ei}\left(-\frac{\gamma_0\lambda_4}{\kappa\lambda_3\lambda}\right)\right\}\right]\frac{d\gamma_0}{1+\gamma_0}.
\tag{27}
$$

Combining Equation (25) with Equation (27), the EE in Case 1 can be obtained as

$$
EE_1^\infty = \frac{\frac{(1-\alpha)}{2\ln 2}\int_0^\infty\left[1-\left\{\frac{\gamma_0\lambda_4\lambda}{\kappa\lambda_3}+\left(\frac{\gamma_0\lambda_4}{\kappa\lambda_3\lambda}\right)^2\exp\left(\frac{\gamma_0\lambda_4}{\kappa\lambda_3\lambda}\right)\mathrm{Ei}\left(-\frac{\gamma_0\lambda_4}{\kappa\lambda_3\lambda}\right)\right\}\right]\frac{d\gamma_0}{1+\gamma_0}}{(1+\mu)P/\varepsilon+P_C}.
\tag{28}
$$

Case 2: $\lambda_1 \neq \lambda_2$.

Similar to Case 1, we can calculate the EE for the exact and the asymptotic analyses, respectively, as follows:

$$
EE_{2\_avg} = \frac{\frac{(1-\alpha)\kappa\lambda_3}{2(\lambda_2-\lambda_1)\ln 2}\int_0^\infty\int_0^\infty \frac{x\exp\left(-\frac{\gamma_0}{\kappa\Delta\lambda_3 x}\right)}{(\kappa\lambda_3 x+\gamma_0\lambda_4)(1+\gamma_0)}\times\left\{\exp\left(-\frac{x}{\lambda_2}\right)-\exp\left(-\frac{x}{\lambda_1}\right)\right\}dxd\gamma_0}{(1+\alpha)P/\varepsilon+P_C}
\tag{29}
$$

$$
EE_{2\_avg}^\infty = \frac{\frac{(1-\alpha)}{2\ln 2}\int_0^\infty\left[1-\left\{\frac{\gamma_0\lambda_4}{\kappa\lambda_3(\lambda_2-\lambda_1)}\left\{\exp\left(\frac{\gamma_0\lambda_4}{\kappa\lambda_3\lambda_1}\right)\mathrm{Ei}\left(-\frac{\gamma_0\lambda_4}{\kappa\lambda_3\lambda_1}\right)-\exp\left(\frac{\gamma_0\lambda_4}{\kappa\lambda_3\lambda_2}\right)\mathrm{Ei}\left(-\frac{\gamma_0\lambda_4}{\kappa\lambda_3\lambda_2}\right)\right\}\right\}\right]\frac{d\gamma_0}{1+\gamma_0}}{(1+\alpha)P/\varepsilon+P_C}
\tag{30}
$$

4. Results and Discussion

In this section, we used the Monte Carlo simulation to verify the accuracy of the analysis expressions from the previous section. For each simulation, we first provided the graphs of the OP and the EE obtained by the analytical formulas. Secondly, we generated plots of the same OP and EE curves that resulted from the Monte Carlo simulation. To do this, we generated 10^5 random samples of each channel gain, which were Rayleigh distributed. The analytical curve and the simulation should match together to verify the accuracy of our analysis [30–33].

In Figure 3, we plotted the effect of the time switching factor α on the OP in two cases—Case 1 and Case 2, respectively. In these cases, we set the primary system parameters as R = {1,3} bps/Hz, Δ = 5 dB, and η = 0.8. From the research results, the OP of the proposed system decreased with increasing α from 0 to 1, and the OP of R = 1 bps/Hz was not better than that with R = 3 bps/Hz. It can be seen that the OP was better with the higher R, and that the OP of Case 2 was better than that of Case 1. Moreover, the OP versus Δ is illustrated in Figure 4 with the exact and asymptotic expressions. In this

case, we set R = 1 bps/Hz and α = 0.5. Similar to Figure 3, we considered two cases, Case 1 and Case 2, in Figure 4. We observed that the OP decreased significantly with increasing Δ from −5 to 15 dB and then converged into the asymptotic OP with Δ from 15 to 25, as shown in Figure 4. Once again, we saw that the OP of Case 2 was better than that of Case 1. From the results in Figures 3 and 4, we can conclude that all the simulation and analytical results are the same for all values of α and Δ.
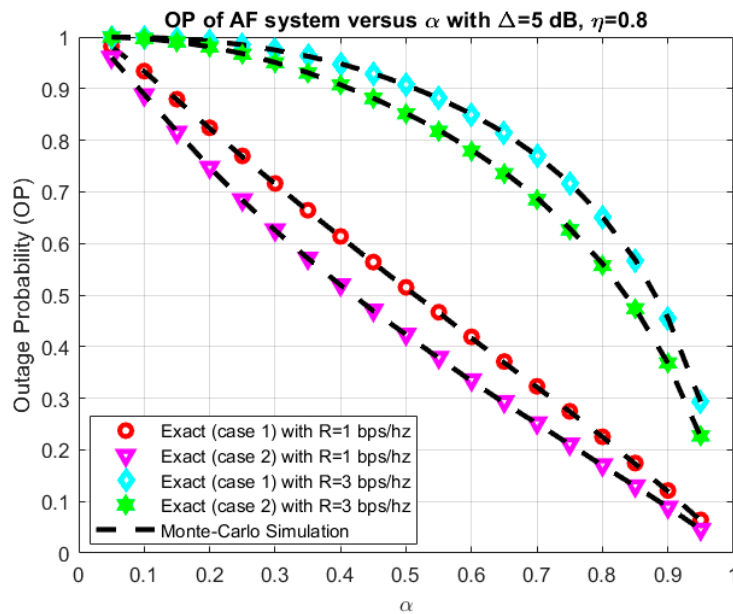
Figure 3. OP versus α. OP, outage probability.
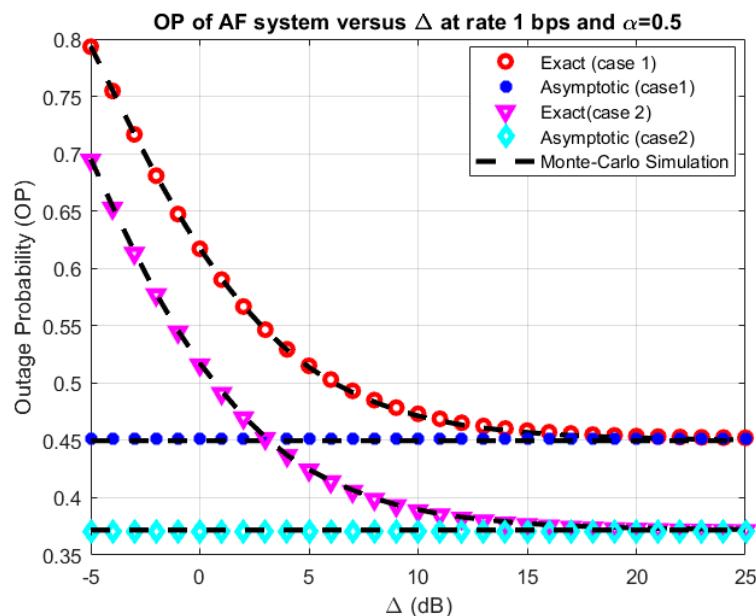
Figure 4. OP versus Δ.

Furthermore, the OP of the model system versus the energy conversion coefficient η of the two cases, Case 1 and Case 2, is shown in Figure 5 with Δ = {1,5} dB, R = 1 bps/Hz and α = 0.5. As the results are the same in the above figures, we determined that the OP of the proposed system decreased crucially while η varied from 0 to 1 and that the OP of Case 2 was better than that of Case 1. Also, all simulation results agreed well with the analytical results with varying η.
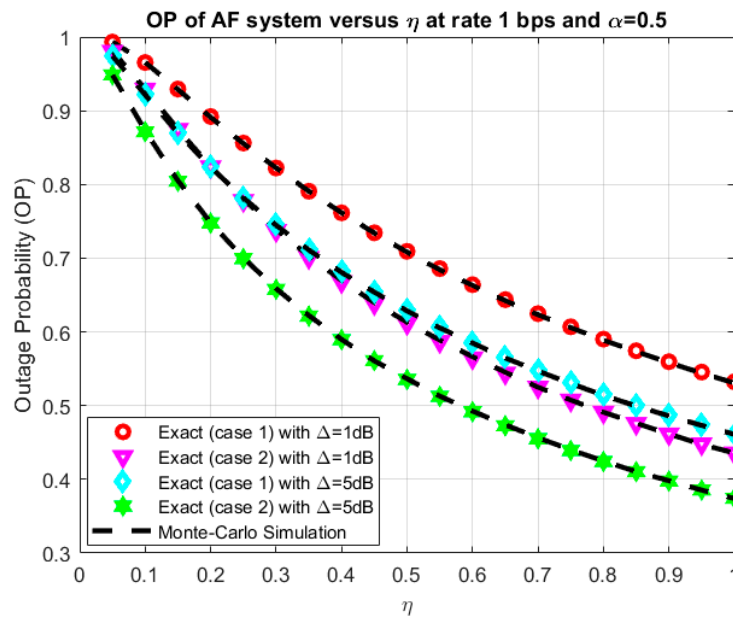
Figure 5. OP versus η.

We investigated the influence of the $\lambda_1 = \lambda_2 = \lambda$ on Case 1 of the OP of the model system, as illustrated in Figure 6. Here, we set $\Delta = \{1,5,10\}$ dB, η = 0.8, α = 0.5, and R = 1 bps/Hz. From the results, we saw that the OP fell with the rising λ, and the OP was better with a higher value of Δ. Moreover, the effect of $\lambda_1 \neq \lambda_2$ on the OP of the model system in connection with λ_1 and λ_2 is presented in Figure 7 with the primary system parameters as $\Delta = \{1,5,10\}$ dB. In this situation, both λ_1 and λ_2 varied from 0 to 4. From the results, we can conclude that the OP of the system falls when λ_1 and λ_2 increase. The optimal value of the system OP was obtained at $\lambda_1 = \lambda_2 = 0$. Finally, we can see that all the simulation and analytical results in Figures 6 and 7 are the same as those in the above section.
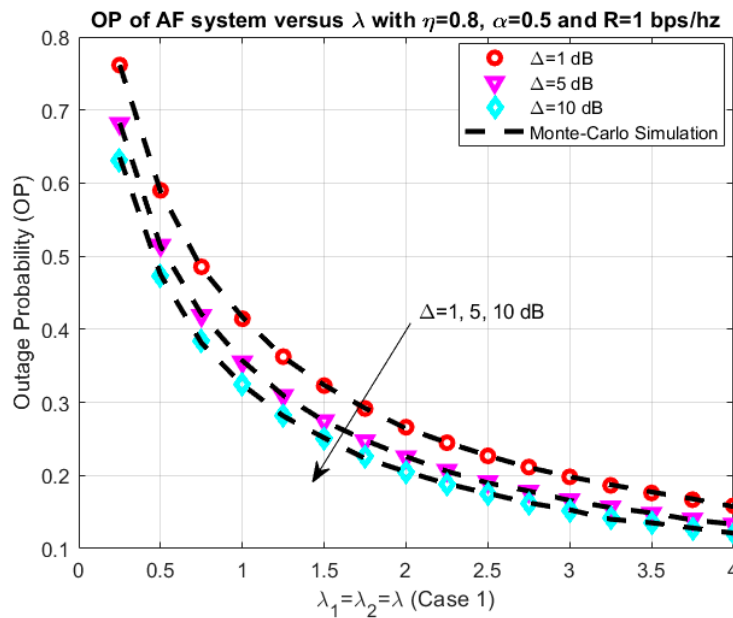
Figure 6. OP versus $\lambda_1 = \lambda_2 = \lambda$.
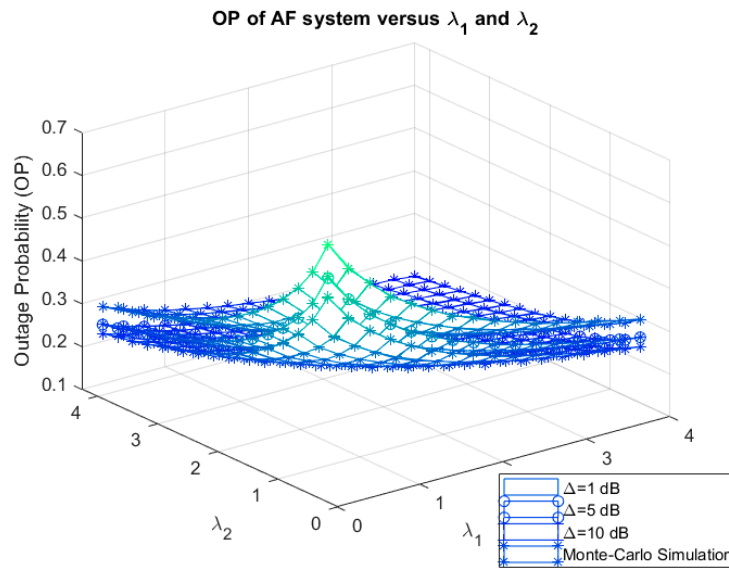
Figure 7. OP versus $\lambda_1 \neq \lambda_2$.

Notably, the EE of the model system versus α is shown in Figure 8 with η = {0.5, 0.85}, R = 1 bps/Hz, Δ = 5 dB, and α varying from 0 to 1. From Figure 8, we can conclude that the EE rises significantly when α rises from 0 to 0.5, after which the EE value decreases. The optimal value of EE could be obtained with α from 0.4 to 0.6. Both Cases 1 and 2 are considered in Figure 8, and it can be observed that the EE of Case 2 is better than that of Case 1 in connection with different values of η. Furthermore, the influence of the circuit power consumption (CPC) on the system EE is presented in Figure 9 with α = {0.5, 0.85}, R = 1 bps/Hz, Δ = 5 dB. In this research, we investigated two cases, Case 1 and Case 2, to validate the exact form expression of the system EE. In Figure 9, it can be seen that the system EE of Case 2 is better than that of Case 1, and the system EE significantly decreases with the increase in the CPC from 0 to 10. Also, the system EE versus Δ is plotted in Figure 10 for both Cases 1 and 2 for exact and asymptotic expressions. Here, we set R = 1 bps/Hz and α = 0.5. From the results, we can conclude that the system exact EE increases with the increase of Δ from −5 to 25 and convergences on the asymptotic values. From all of the Figures 8–10, we can conclude that the simulation verifies the analytical results completely.
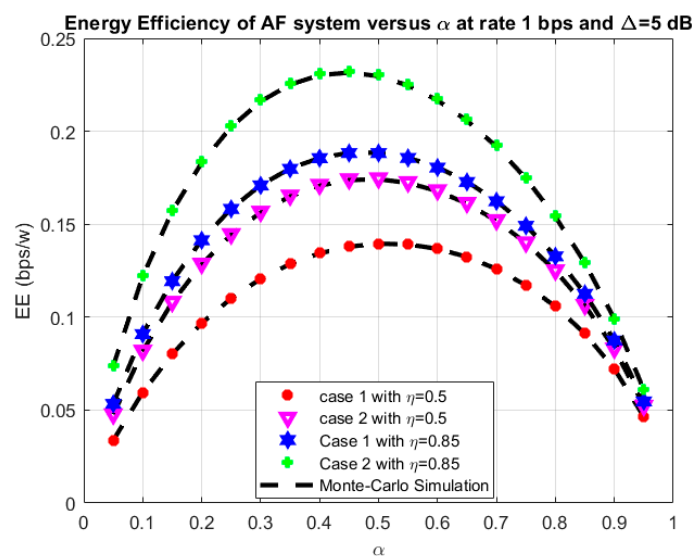
Figure 8. Energy efficiency (EE) versus α.
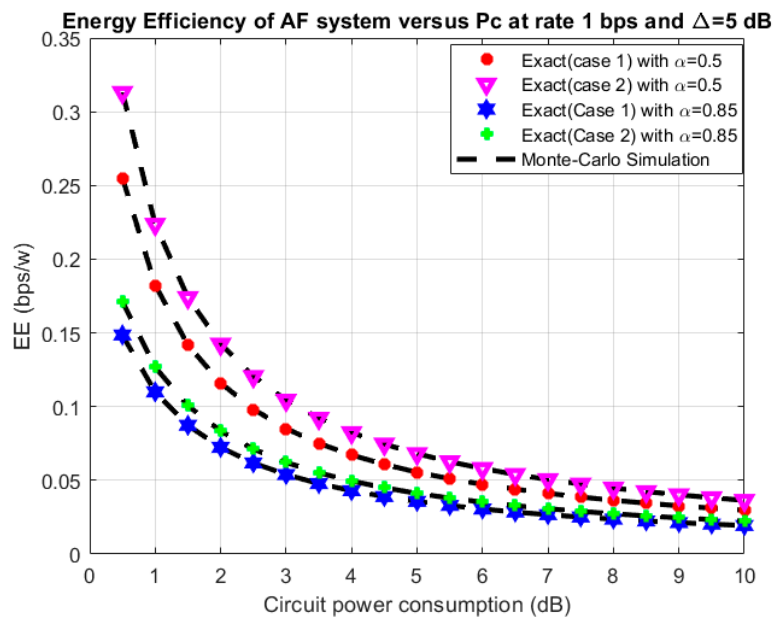
Figure 9. EE versus circuit power consumption (CPC).
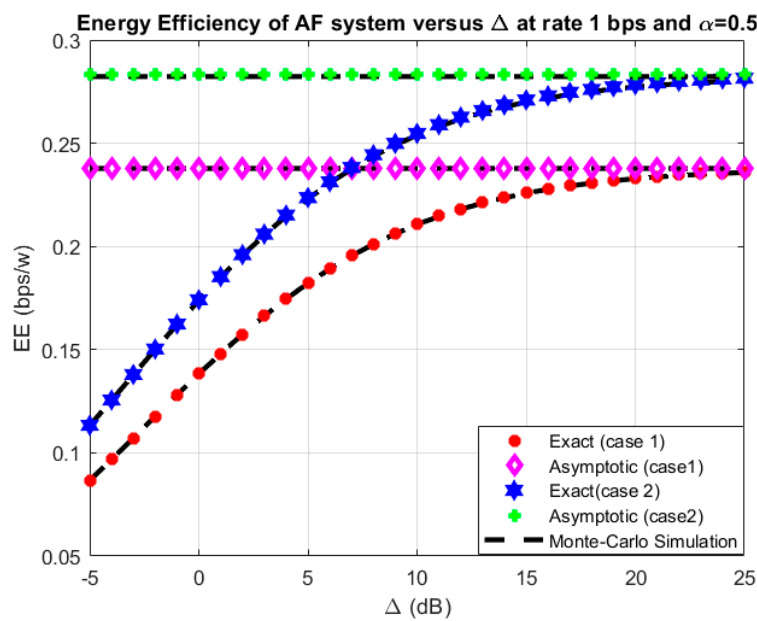
Figure 10. EE versus Δ.

5. Conclusions

In this paper, we investigated the PB EH in an HD communication network under co-channel interference over a Rayleigh fading environment. We considered the model system in the TS protocol. Firstly, the exact and asymptotic form expressions of the OP were derived. Then we investigated the EE of the model system and the influence of the primary system parameters on the performance of the proposed system. Finally, the accuracy of the analytical expressions was derived and verified using a Monte Carlo simulation in connection with the primary system parameters. From the results, we can conclude that the analytical mathematical and simulated results are the same, thus verifying the correctness of the analytical expressions.

Author Contributions: Methodology, V.-D.P., T.T.T.; software, T.N.N., D.-H.H., V.-D.P., T.-L.N.; validation, T.T.T., V.-D.P., D.-H.H., T.-L.N.; Writing—original draft preparation, T.N.N., M.T.; writing—review and editing, T.N.N., M.T.; supervision, M.V.

Conflicts of Interest: The authors declare no conflict of interest.

References

1. Wong, K.D. *Fundamentals of Wireless Communication Engineering Technologies*; John Wiley and Sons: Hoboken, NJ, USA, 2011. [CrossRef]

2. Bi, S.; Ho, C.K.; Zhang, R. Wireless powered communication: Opportunities and challenges. *IEEE Commun. Mag.* **2015**, *53*, 117–125. [CrossRef]

3. Niyato, D.; Kim, D.I.; Maso, M.; Han, Z. Wireless Powered Communication Networks: Research Directions and Technological Approaches. *IEEE Wirel. Commun* **2017**, *24*, 2–11. [CrossRef]

4. Yu, H.; Lee, H.; Jeon, H. What is 5G? Emerging 5G Mobile Services and Network Requirements. *Sustainability* **2017**, *9*, 1848. [CrossRef]

5. Nguyen, T.N.; Tran, M.; Nguyen, T.-L.; Ha, D.-H.; Voznak, M. Performance Analysis of a User Selection Protocol in Cooperative Networks with Power Splitting Protocol-Based Energy Harvesting Over Nakagami-m/Rayleigh Channels. *Electronics* **2019**, *8*, 448. [CrossRef]

6. Bi, S.; Ho, C.K.; Zhang, R. Recent Advances in Joint Wireless Energy and Information Transfer. In Proceedings of the 2014 IEEE Information Theory Workshop (ITW2014), Hobart, TAS, Australia, 2–5 November 2014. [CrossRef]

7. Kawabata, H.; Ishibashi, K. RF Energy Powered Feedback-aided Cooperation. In Proceedings of the 2014 IEEE 25th Annual International Symposium on Personal, Indoor, and Mobile Radio Communication (PIMRC), Washington, DC, USA, 2–5 September 2014. [CrossRef]

8. Huang, K.; Lau, V.K.N. Enabling Wireless Power Transfer in Cellular Networks: Architecture, Modeling and Deployment. *IEEE Trans. Wirel. Commun.* **2014**, *13*, 902–912. [CrossRef]

9. Medepally, B.; Mehta, N.B. Voluntary Energy Harvesting Relays and Selection in Cooperative Wireless Networks. *IEEE Trans. Wirel. Commun.* **2010**, *9*, 3543–3553. [CrossRef]

10. Zhou, X.; Zhang, R.; Ho, C.K. Wireless Information and Power Transfer: Architecture Design and Rate-energy. *IEEE Trans. Commun. (GLOBECOM)* **2013**, *61*, 4754–4761. [CrossRef]

11. Liu, L.; Zhang, R.; Chua, K.C. Wireless Information and Power Transfer: A Dynamic Power Splitting Approach. *IEEE Trans. Commun.* **2013**, *61*, 3990–4001. [CrossRef]

12. Nasir, A.A.; Zhou, X.; Durrani, S.; Kennedy, R.A. Relaying Protocols for Wireless Energy Harvesting and Information Processing. *IEEE Trans. Wirel. Commun.* **2013**, *12*, 3622–3636. [CrossRef]

13. Peng, C.L.; Li, F.W.; Liu, H. Optimal Power Splitting in Two-Way Decode-and-Forward Relay Networks. *IEEE Commun. Lett.* **2017**, *21*, 2009–2012. [CrossRef]

14. Tan, N.; Nguyen, T.H.Q.; Minh, P.; Tran, T. Miroslav Voznak. Energy Harvesting over Rician Fading Channel: A Performance Analysis for Half-Duplex Bidirectional Sensor Networks under Hardware Impairments. *Sensors* **2018**, *18*, 1781.

15. Do, D.T.; Van Nguyen, M.S.; Hoang, T.A.; Voznak, M. NOMA-Assisted Multiple Access Scheme for IoT Deployment: Relay Selection Model and Secrecy Performance Improvement. *Sensors* **2019**, *19*, 736. [CrossRef]

16. Do, D.T.; Le, C.B. Application of NOMA in Wireless System with Wireless Power Transfer Scheme: Outage and Ergodic Capacity Performance Analysis. *Sensors* **2018**, *18*, 3501. [CrossRef]

17. Zhou, X.; Li, Q. Energy Efficiency for SWIPT in MIMO Two-Way Amplify-and-Forward Relay Networks. *IEEE Trans. Veh. Technol.* **2018**, *67*, 4910–4924. [CrossRef]

18. Lu, G.; Lei, C.; Ye, Y.; Shi, L.; Wang, T. Energy Efficiency Optimization for AF Relaying with TS-SWIPT. *Energies* **2019**, *12*, 993. [CrossRef]

19. Nguyen, X.X.; Do, D. Optimal power allocation and throughput performance of full-duplex DF relaying networks with wireless power transfer-aware channel. *EURASIP J. Wirel. Commun. Netw.* **2017**, 152. [CrossRef]

20. Masood, Z.; Jung, S.P.; Choi, Y. Energy-Efficiency Performance Analysis and Maximization Using Wireless Energy Harvesting in Wireless Sensor Networks. *Energies* **2018**, *10*, 2917. [CrossRef]

21. Ng, D.W.K.; Lo, E.S.; Schober, R. Wireless Information and Power Transfer: Energy Efficiency Optimization in OFDMA Systems. *IEEE Trans. Wirel. Commun.* **2013**, *12*, 6352–6370. [CrossRef]

22. Nguyen, T.N.; Tran, M.; Nguyen, T.-L.; Ha, D.-H.; Voznak, M. Multisource Power Splitting Energy Harvesting Relaying Network in Half-Duplex System over Block Rayleigh Fading Channel: System Performance Analysis. *Electronics* **2019**, *8*, 67. [CrossRef]

23. Zhang, J.; Haardt, M. Energy Efficient Two-Way Non-Regenerative Relaying for Relays with Multiple Antennas. *IEEE Signal Process. Lett.* **2015**, *22*, 1079–1083. [CrossRef]

24. Zappone, A.; Bjornson, E.; Sanguinetti, L.; Jorswieck, E. Globally Optimal Energy-Efficient Power Control and Receiver Design in Wireless Networks. *IEEE Trans. Signal Process.* **2017**, *65*, 2844–2859. [CrossRef]

25. Huang, Y.; Liu, M.; Liu, Y. Energy-Efficient SWIPT in IoT Distributed Antenna Systems. *IEEE Internet Things J.* **2018**, *8*, 2646–2656. [CrossRef]

26. Chen, X.; Wang, X.; Chen, X. Energy-Efficient Optimization for Wireless Information and Power Transfer in Large-Scale MIMO Systems Employing Energy Beamforming. *IEEE Wirel. Commun. Lett.* **2013**, *2*, 667–670. [CrossRef]

27. Guo, S.; Yang, Y.; Yu, H. Energy-Efficient Cooperative Transmission for SWIPT in Wireless Sensor Networks. In *Wireless Power Transfer Algorithms, Technologies and Applications in Ad Hoc Communication Networks*; Springer: Cham, Switzerland, 2016; pp. 253–281.

28. Mao, S.; Leng, S.; Hu, J.; Yang, K. Energy-Efficient Resource Allocation for Cooperative Wireless Powered Cellular Networks. In Proceedings of the 2018IEEE International Conference on Communications (ICC), Kansas City, MO, USA, 20–24 May 2018.

29. Zwillinger, D. *Table of Integrals, Series, and Products*; Elsevier Science: Amsterdam, The Netherlands, 2014. [CrossRef]

30. Nguyen, T.N.; Minh, T.H.Q.; Tran, P.T.; Voznak, M. Tran and Miroslav Voznak. Adaptive Energy Harvesting Relaying Protocol for Two-Way Half Duplex System Network over Rician Fading Channel. *Wirel. Commun. Mob. Comput.* **2018**, *2018*, 7693016. [CrossRef]

31. Bhatnagar, M.R. On the Capacity of Decode-and-Forward Relaying over Rician Fading Channels. *IEEE Commun. Lett.* **2013**, *17*, 1100–1103. [CrossRef]

32. Nguyen, T.N.; Minh, T.H.Q.; Tran, P.T.; Voznak, M.; Duy, T.T.; Nguyen, T.-L.; Tin, P.T. Performance enhancement for energy harvesting based two-way relay protocols in wireless ad-hoc networks with partial and full relay selection methods. *Ad Hoc Networks* **2019**, *84*, 178–187. [CrossRef]

33. Nguyen, T.N.; Tran, M.; Ha, D.-H.; Nguyen, T.-L.; Voznak, M. Energy harvesting based two-way full-duplex relaying network over a Rician fading environment: performance analysis. *Proceedings of the Estonian Academy of Sciences* **2019**, *68*, 111. [CrossRef]